Agricultural and Forest Meteorology 333 (2023) 109386

Contents lists available at ScienceDirect

Agricultural and Forest Meteorology

journal homepage: www.elsevier.com/locate/agrformet

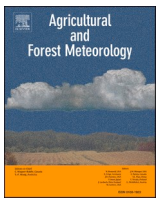

Estimating source-sink distributions and fluxes of reactive nitrogen and sulfur within a mixed forest canopy

Zhiyong Wu [a,1], John T. Walker [b,*], A. Christopher Oishi [c], Tomer Duman [d], Gabriel Katul [e], Xi Chen [b,2], Donna Schwede [b], Jesse Bash [b], John Iiames [b]

[a] ORISE Fellow at the Office of Research and Development, US Environmental Protection Agency, Durham, NC, United States
[b] Office of Research and Development, US Environmental Protection Agency, Durham, NC, United States
[c] Southern Research Station, Coweeta Hydrologic Laboratory, USDA Forest Service, Otto, NC, United States
[d] Department of Biology, The University of New Mexico, Albuquerque, NM, United States
[e] Department of Civil and Environmental Engineering, Duke University, Durham, NC, United States

ARTICLE INFO

Keywords:
Inverse model
Reactive nitrogen
Reactive sulfur
Source-sink
Turbulent flux profile

ABSTRACT

The vertical source-sink distribution of air pollutants within and above forested canopies is necessary for describing the biological, physical, and chemical processes influencing the soil-vegetation-atmosphere exchange. This study implemented inverse modeling methods to estimate the source-sink and flux profiles of reactive nitrogen (N) and sulfur (S) compounds from measurements of the mean concentration profiles of ammonia (NH_3), nitric acid (HNO_3), sulfur dioxide (SO_2), and particulate ammonium (NH_4^+), nitrate (NO_3^-), and sulfate (SO_4^{2-}) at a forest site in the southern Appalachian Mountains. Three inverse approaches utilizing different approximations to scalar transport within the canopy were developed and evaluated against sensible heat flux measurements. The Eulerian model (EUL), which incorporates vertical velocity skewness, performed well in reproducing the turbulent heat fluxes and was subsequently used to calculate the chemical source-sink and flux profiles. Above-canopy fluxes of NH_3 were downward, indicating that the forest was a net sink of NH_3. The soil/litter layer was both a source and a sink for NH_3 but the exchange rate at the forest floor was small. Fluxes of HNO_3, SO_2, NO_3^-, NH_4^+, and SO_4^{2-} were uni-directional (deposition only) between the air and the canopy/ground and increased monotonically from the forest floor to the canopy top. Crown foliage dominated the uptake of reactive N and S during the growing season, accounting for 80–90% of the total canopy-scale flux. Fluxes and canopy-ground partitioning estimated using the resistance-based Surface Tiled Aerosol and Gas Exchange (STAGE) model were generally comparable to EUL. The comparison highlights the need for improved parameterizations of litter exchange and NH_3 compensation points in resistance models for forest ecosystems. The findings here benefit the application of critical loads in forest ecosystems and guide further development of resistance-based exchange models.

1. Introduction

Quantifying biosphere-atmosphere exchange of reactive compounds is necessary for assessing air pollution and climate change impacts on human and ecosystem health and for understanding global biogeochemical cycles (Fowler et al., 2009; Massad and Loubet, 2015). Air concentrations monitored by regional and continental networks (e.g., CASTNET, CAPMoN, NitroEurope) have been combined with inferential modeling to provide long-term estimates of the canopy-scale mass exchange of reactive compounds. However, the within-canopy distribution of sources and sinks of reactive compounds remains uncertain, which limits characterization of the key exchange processes and the improvement of generalized resistance-based exchange models.

Estimation of the scalar turbulent flux profile within vegetation canopies is challenging due to the presence of vertically distributed sources and sinks (biological or chemical). The near-field effect of these variable sources and sinks often results in the failure of conventional flux-gradient techniques (also known as “K-theory”) within the canopy

* Corresponding author.
E-mail address: Walker.Johnt@epa.gov (J.T. Walker).
[1] Now at RTI International, Durham, NC, USA.
[2] Now at Office of Air Quality Planning and Standards, US Environmental Protection Agency, Durham, NC, USA.

https://doi.org/10.1016/j.agrformet.2023.109386
Received 24 June 2022; Received in revised form 8 February 2023; Accepted 20 February 2023
Available online 13 March 2023
0168-1923/Published by Elsevier B.V.

(Denmead et al., 2008; Harper et al., 2000; Raupach, 1988). Efforts to circumvent the limitation of "K-theory" have led to the development of two alternative approaches: Lagrangian dispersion models (including the localized near-field theory and stochastic trajectory models) and higher-order Eulerian closure models (Katul and Albertson, 1999). In both approaches, scalar source/sink density (S) and turbulent flux (F) distribution with distance z from the ground can be inferred from the mean scalar concentration profiles (i.e., mean air temperature, mean water vapor concentration, mean carbon dioxide concentration, etc.…) above and within the canopy if certain flow statistics are known (measured or modeled). This problem of inferring sources/sinks and turbulent fluxes from measured mean concentration profiles is commonly referred to as "inverse source-sink modeling" (Katul and Albertson, 1999; Raupach, 1989a). Both Eulerian and Lagrangian models assume vertical transport only (with no horizontal dispersion) and planar-homogeneous turbulence. The simplified Lagrangian models do not include nonzero vertical velocity skewness, strong inhomogeneity in vertical source strength, and advective transport (Katul and Albertson, 1999). While the Eulerian models circumvent some of those limitations, they are sensitive to measurement errors in concentration due to the lack of redundancy in the inversion for source/sink strength from measured concentrations (Siqueira et al., 2000). As each of these models is subject to different assumptions and limitations, it is worthwhile to inter-compare and evaluate their various forms to constrain the calculated source/sink scalar strength distribution and permit multiple inferences on the origin and fate of reactive compounds within the canopy.

The motivation for using such "inverse source-sink modeling" is the complexity of the atmospheric chemistry and biosphere-atmosphere interactions in the southern Appalachian Mountains. The southern Appalachian Mountains encompass biomes that are sensitive to acidic and nitrogen deposition and have been the target of the Southern Appalachian Nitrogen Deposition Study (SANDS) conducted in 2015 and 2016 at the Coweeta Hydrologic Laboratory in southwest North Carolina. Walker et al., 2023 developed a complete annual reactive nitrogen deposition budget for Coweeta Forest by combining measurements with canopy-scale "big leaf" resistance modeling. This paper extends the budget analysis of Walker et al., 2023 to examine the within-canopy exchange processes of reactive N and S using an alternative non-resistance-based modeling approach. Here, the vertical distribution of the source/sink density and chemical fluxes is derived from measured profiles of scalar concentrations and turbulent flow statistics within and above the same canopy by implementing inverse models. The sources/sinks and fluxes of reactive N and S compounds are partitioned to specific ecosystem compartments (e.g., crown, understory, ground), and then compared with the fluxes and partitioning estimated from a resistance-based exchange model (i.e., the Surface Tiled Aerosol and Gaseous Exchange (STAGE) model; Walker et al., 2023).

Three common inverse models were tested to estimate the source/sink and flux distributions within the canopy: a Eulerian higher-order closure model (EUL) (Katul and Albertson, 1999), a Lagrangian localized near-field (LNF) model (Katul et al., 1997; Raupach, 1989a), and a new full Lagrangian stochastic model (LSM) (Duman et al., 2016). The manuscript is organized as follows: Section 2 describes the measurements and the framework and formulations of the inverse models. Next, the inverse models are implemented to calculate the profiles of sensible heat flux within the canopy and the results are compared against multi-level eddy covariance measurements (Section 3). The best performing inverse model is then used to derive height-resolved source/sink and chemical fluxes of reactive nitrogen and sulfur compounds within the canopy, followed by analysis and comparison with the resistance-based model formulation in Section 4. A summary of major findings and recommendations are provided in Section 5.

2. Methodology

2.1. Site description

These experiments were conducted as part of the SANDS field campaign (Walker et al., 2023) in the Coweeta Hydrologic Laboratory. The site (hereafter referred to as Coweeta Forest) is located in a ~90 year-old mixed broadleaf deciduous hardwood forest in the southern Appalachian Mountains of southwest North Carolina (35°4′N, 83°26′W; elevation 690 m). The canopy is dominated by black birch (*Betula lenta* L.), tulip poplar (*Liriodedron tulipifera* L.), white oak (*Quercus alba* L.), and red maple (*Acer rubrum* L.). The understory consists of evergreen shrubs such as rosebay rhododendron (*Rhododendron maximum* L.), which comprises 15% of basal area and can reach over 4 m in height (Oishi et al., 2018). A walk-up tower is used as the main structure supporting instruments to measure the scalar concentration profiles, eddy covariance fluxes, and related meteorological variables. The height of the tower was extended on May 20, 2016 from 37.0 m to 43.5 m. The terrain within the flux footprint of the tower is complex, characterized by a 30% slope in the southeast direction and local slopes of <10% to the northeast and southwest (Novick et al., 2014). During the sampling period, the predominant winds were from the northeast and southwest as discussed in the supplementary material (Fig. S1). The canopy height near the tower is approximately 30 m with a peak one-sided leaf area index (LAI) of 4.6 $m^2\ m^{-2}$ during the growing season (Oishi et al., 2018).

2.2. Data collection and quality control

2.2.1. Chemical concentration profiles

Between May 2015 and August 2016, five intensive field experiments were conducted at Coweeta Forest to obtain the concentration profiles for reactive nitrogen and sulfur compounds (Table S1). Concentrations of nitric acid (HNO_3), ammonia (NH_3), sulfur dioxide (SO_2), nitrate (NO_3^-), ammonium (NH_4^+), and sulfate (SO_4^{2-}) in air were measured concurrently at 10 heights from just above the forest floor (0.53 m above ground) to several meters above the canopy (37.65 m during the first four intensive experiments, 43.00 m during the last intensive experiment) using a glass annular denuder/filter pack (URG Corporation, Chapel Hill, NC) system. The eight sampling heights in the middle were 1.78, 4.42, 9.91, 17.23, 24.85, 28.20, 32.01, and 34.60 m above ground, respectively. The sampling assembly included a 1% Na_2CO_3 coated denuder for collection of acid gasses followed by a 1% H_3PO_3 coated denuder for collection of NH_3, and a filter pack containing a primary Teflon filter for collection of aerosol and a backup Nylon filter (47 mm, Pall Corp, Port Washington, NY) to collect HNO_3 liberated by dissociation of NH_4NO_3 on the primary filter. Inlets were Teflon coated glass impactors with a nominal 2.5 μm aerodynamic diameter cutpoint (URG Corporation, Chapel Hill, NC). Sampling durations were typically 3 or 4 h at a flow rate of about 16.7 L min^{-1}. Flow rates were controlled by critical orifice and were checked before and after each sampling period with a NIST traceable primary standard flow meter (Bios DryCal DC-Lite flowmeter, Mesa Laboratories, Inc., Lakewood, CO).

Denuders and filters were extracted with 10 mL of deionized water and analyzed by ion chromatography (IC, Dionex model ICS-2100, Thermo Scientific, Waltham, MA). Extracts were analyzed for cations using Dionex IonPac 2 mm CG12 guard and CS12 analytical columns; separations were conducted using 20 mM methanesulfonic acid (MSA) as eluent at a flow rate of 0.25 mL min^{-1}. Anions were analyzed (IonPac 2 mm AG23 guard column, AS23 analytical columns) using an isocratic eluent mix of carbonate/bicarbonate (4.5/0.8 mM) at a flow rate of 0.25 mL min^{-1}. Multi-point (≥5) calibrations were conducted using a mixture prepared from individual inorganic standards (Inorganic Ventures, Christiansburg, VA). A mid-level accuracy check standard was prepared from certified standards mix (AccuStandard, New Haven, CT) for quality assurance/quality control.

Field blanks were sampled in the intensive experiments and analyzed

in the lab using the same procedures as the normal samples. Following Currie (1995), the detection limits for each species were calculated as the standard deviation of concentrations for the field blanks and are listed in Table S2. Duplicate samples were taken at the lowest and highest levels and the scatter plots are shown in the left panels of Figs. S2 – S7. The relative measurement errors were calculated as the relative deviation from the mean: (C_i - C_{mean}) / C_{mean}× 100%, where C_i is concentration of the duplicate sample #1 or #2 and C_{mean} is the mean concentration of the two duplicate samples (see the right panels of Figs. S2 – S7).

2.2.2. Eddy covariance and micrometeorology

Three-dimensional wind velocity components along with momentum and sensible heat fluxes were measured at seven levels (2.0, 4.0, 9.4, 16.8, 24.1, 29.6, and 37.65/43.5 m) throughout the canopy. The subcanopy sonic anemometer (Model 81000, R.M. Young Company, Traverse City, MI) at 2.0 m above the forest ground was located approximately 35 m southwest of the tower and the other six (Model 81000, R.M. Young Company, Traverse City, MI) were installed on the tower. Ecosystem fluxes of carbon dioxide and water vapor were estimated using the sonic anemometer above the canopy (43.5 m) and a co-located closed path infrared gas analyzer (EC155, Campbell Scientific, Logan, UT). The subcanopy sonic anemometer coupled with an open path infrared gas analyzer (LI-7500, LI-COR, Lincoln, NE) were used to estimate the carbon dioxide and water vapor fluxes from the soil and herbaceous vegetation. The sampling frequency was 10 Hz for the subcanopy and above-canopy eddy covariance systems and 5 Hz for the five anemometers in the middle. The raw 5 and 10 Hz data were processed into hourly averages after block average detrending, 2D-coordinate rotation, and correction for spectral attenuation and density fluctuations. Detailed information on instrument and data processing methods can be found elsewhere (Novick et al., 2013; Oishi et al., 2018).

The mean temperature profiles were measured at 4.0, 9.4, 16.8, 24.1, 29.6, and 43.5 m above the forest ground using aspirated thermocouples (ASPTC, Campbell Scientific, Logan, UT). Common biometeorological variables including air temperature, relative humidity, pressure, wind speed and direction, solar radiation, and precipitation rate were recorded at the top of the tower. Soil temperature was measured at four depths (5, 20, 35, and 55 cm) in two locations near the tower using thermistors. Soil volumetric water content averaged over 0–30 cm depth was measured in four locations around the tower using time domain reflectometry probes (CS616, Campbell Scientific).

2.3. Description of the inverse models

Three common methods for inverse modeling of the source/sink distribution within the canopy are compared including a Eulerian second-order closure model (EUL) (Katul and Albertson, 1999), a Lagrangian localized near-field (LNF) model (Raupach, 1989a, 1989b), and a Lagrangian stochastic trajectory model (LSM) (Duman et al., 2016). Each method has its own assumptions and requires different aspects of the flow field and/or timescale. In this section, the key equations in the models are briefly described.

2.3.1. Eulerian closure model (EUL)

In the Eulerian framework, the effective source/sink strength (S) of scalar c is estimated from the steady state mean scalar conservation equation (Finnigan, 1985; Raupach, 1988):

$$-\frac{\partial \overline{w'c'}}{\partial z} + S = 0, \tag{1}$$

where the turbulent flux $\overline{w'c'}$ is estimated from the corresponding flux budget equation:

$$\frac{\partial \overline{w'c'}}{\partial t} = 0 = -\overline{w'w'}\frac{\partial \overline{c}}{\partial z} - \frac{\partial \overline{w'w'c'}}{\partial z} - \overline{c'\frac{\partial p'}{\partial z}}, \tag{2}$$

with the following closure models employed (Katul and Albertson, 1999; Meyers, 1987):

$$\overline{w'w'c'} = \frac{\tau}{C_8}\left(-\overline{w'w'w'}\frac{\partial \overline{c}}{\partial z} - \overline{w'c'}\frac{\partial \overline{w'w'}}{\partial z} - 2\overline{w'w'}\frac{\partial \overline{w'c'}}{\partial z}\right), \tag{3}$$

$$\overline{c'\frac{\partial p'}{\partial z}} = C_4\frac{\overline{w'c'}}{\tau}. \tag{4}$$

Here, S must be interpreted as a net source or sink at height z and includes all the physical (e.g. deposition), biological (emission or uptake from plant area density at height z), or chemical transformations leading to the generation or destruction of scalar c at height z, c is the scalar concentration (or temperature in the case of heat transport), w is the vertical velocity, z is height, p is the deviation from static pressure, τ is a Eulerian time scale, and C_4 and C_8 are the two closure constants. Primes denote fluctuations from time averages (represented by overbars). Dispersive fluxes arising from the need to spatially average the time-averaged equations are ignored. The closure in Eq. (4) also ignores the contribution of rapid terms (known as isotropization of the production terms) for simplicity, though these terms can be incorporated in the inversion should it be necessary. The inclusion of an isotropization of production correction to Eq. (4) necessitates measurements or models of the covariances between air temperature and scalar concentration fluctuations, which are far less studied or understood. For this reason, only the slow-part (i.e. the classical Rotta term) is accounted for.

To derive the flux profile from the mean concentration profile, Eqs. (3) and (4) are combined with (2). Thus, the Eulerian closure model (EUL) can be derived as follows (Katul and Albertson, 1999):

$$A_1(z)\frac{\partial^2 \overline{w'c'}}{\partial z^2} + A_2(z)\frac{\partial \overline{w'c'}}{\partial z} + A_3(z)\overline{w'c'} = A_4(z) \tag{5}$$

where

$$A_1(z) = \frac{2\tau}{C_8}\overline{w'w'},$$

$$A_2(z) = \frac{\tau}{C_8}\frac{\partial \overline{w'w'}}{\partial z} + 2\frac{\partial}{\partial z}\left(\frac{\tau}{C_8}\overline{w'w'}\right),$$

$$A_3(z) = \frac{\partial}{\partial z}\left(\frac{\tau}{C_8}\frac{\partial \overline{w'w'}}{\partial z}\right) - \frac{C_4}{\tau},$$

$$A_4(z) = \overline{w'w'}\frac{\partial \overline{c}}{\partial z} - \frac{\partial}{\partial z}\left(\frac{\tau}{C_8}\overline{w'w'w'}\right)\frac{\partial \overline{c}}{\partial z} - \left(\frac{\tau}{C_8}\overline{w'w'w'}\right)\frac{\partial^2 \overline{c}}{\partial z^2}$$

The two boundary conditions for Eq. (5) are:

$$z \geq h_c : \overline{w'c'} = \frac{A_4(h_c)}{A_3(h_c)},\ z = 0 : \frac{\partial \overline{w'c'}}{\partial z} = 0,$$

where h_c is the canopy height. It is to be noted that (i) $A_4(z)$ contains all the information about the measured mean scalar concentration profile, and (ii) the relation between turbulent fluxes and mean scalar concentration gradient is 'non-local' because $A_1(z)$ and $A_2(z)$ are finite. That is, the turbulent flux at a single height z requires double integration of Eq. (5) and is thus impacted by the mean concentration values at all z.

2.3.2. Lagrangian frame models (LNF and LSM)

In the Lagrangian framework, the effective source/sink strength (S_j) at layers j = 1,2, …, m is computed according to:

$$c_i - c_R = \sum_{j=1}^{m} D_{ij}S_j dz_j \tag{6}$$

where m is the highest source/sink layer (e.g., canopy top), c_i is the scalar concentration at a given level i, c_R is the concentration at a reference height well above the canopy, D_{ij} is a dispersion kernel, and dz_j is the depth of the layer j. LNF and LSM adopt different approaches to compute the dispersion matrix D_{ij}. However, once D_{ij} is known, the source/sink profile (S_j) can be determined using the measured concentration profile based on Eq. (6).

Raupach (1989b) proposed a localized near field (LNF) theory that the scalar concentration at any point in the canopy is a superposition of near-field and far-field contributions:

$$c(z) = c_n(z) + c_f(z). \tag{7}$$

The near-field component (c_n) does not obey gradient diffusion and is calculated from a one-dimensional probability distribution of concentration:

$$c_n(z) = \int_0^{\infty} \frac{S(z_0)}{\sigma_w(z_0)} \left[k_n\left(\frac{z - z_0}{\sigma_w(z_0)T_L(z_0)}\right) + k_n\left(\frac{z + z_0}{\sigma_w(z_0)T_L(z_0)}\right)\right] dz_0, \tag{8}$$

where σ_w is the standard deviation of vertical velocity, T_L is the Lagrangian integral timescale, and z_0 is the height of the given source. k_n is a near-field kernel function for which an analytical approximation is given by:

$$k_n(x) = -0.39894\ln\left(1 - e^{-|x|}\right) - 0.15623e^{-|x|}. \tag{9}$$

The far-field component (c_f) assumes gradient diffusion and can be calculated using the result from near-field and a gradient-diffusion relation:

$$c_f(z) = c(z_R) - c_n(z_R) + \int_z^{z_R} \frac{\overline{w'c'}}{K_f(z)} dz, \tag{10}$$

where z_R is the reference height. By neglecting the vertical velocity skewness, the far-field diffusivity K_f can be approximated as

$$K_f(z) = \sigma_w^2(z)T_L(z). \tag{11}$$

In the inverse LNF problem, the dispersion matrix D_{ij} can be computed from the calculated concentration (c_i) using Eqs. (7-11) by placing a unit source at layer j if the turbulent flow statistics and the Lagrangian timescale are known (such as from multi-layer sonic measurements).

In the LSM, the dispersion matrix D_{ij} is calculated from a full Lagrangian stochastic scheme (Duman et al., 2016) based on the flow field, taking into account the covariance between vertical (w') and horizontal (u') velocity components. Rather than using an analytical function to represent a concentration profile (as in the LNF), simulated fluid elements are released from each source layer, followed by a calculation of their trajectories. The trajectories are determined by solving a system of Langevin type stochastic differential equations (Rodean, 1996; Thomson, 1987) of the form:

$$du_i = a_i dt + b_{ij} dW_j, \tag{12}$$

where du_i is the change in Lagrangian instantaneous fluid velocity fluctuations along direction i = 1, 2, and 3 and dW_j is the Wiener increment along direction j = 1, 2, and 3 sampled randomly from a zero mean Gaussian distribution with variance dt for each direction independently. Here directions i = 1, 2, and 3 correspond to longitudinal (or x), lateral (or y), and vertical (or z), respectively. The coefficients a and b are calculated as functions of the Eulerian flow statistics (including variances and covariances between velocity components but no third-order statistics), u_i, and a (phenomenological) constant C_0 related to the Lagrangian Kolmogorov constant. Duman et al. (2016) improved the calculations by replacing the mean dissipation with a time-dependent dissipation that is lognormally distributed to account for intermittency effects within the canopy. The particles disperse due to stochastic sampling of the fluid turbulent field, and their trajectories are used to calculate concentration profiles that implicitly include the near-field, far-field, and a transition.

2.4. Model configurations

Besides the concentration profile, the EUL model requires inputs of vertical velocity variance ($\overline{w'w'}$), vertical velocity skewness ($\overline{w'w'w'}$), a Eulerian decorrelation timescale (τ), and two constants (C_4, C_8). LNF requires$\overline{w'w'}$ and a Lagrangian timescale (T_L). For LSM, the velocity variances ($\overline{u'u'}$, $\overline{w'w'}$), Reynolds stress ($\overline{u'w'}$), mean flow velocity ($\overline{u}$), and a Lagrangian time scale (T_L) are needed. The flow statistics were estimated from the high-frequency sonic anemometry measurements at the seven levels and were fitted with similarity theory relations. The flow was averaged over the entire time of measuring the concentration of reactive compounds. The Eulerian integral timescale was determined from the auto-correlation of vertical velocity fluctuation (w') using (Katul et al., 1997)

$$\tau = \int_0^{\infty} \rho_E(s) ds, \tag{13}$$

where $\rho_E(s)$ is the Eulerian vertical velocity auto-correlation function. The Lagrangian timescale was estimated from the Eulerian timescale by approximating

$$T_L = \frac{\overline{u}}{\sigma_w}\tau \tag{14}$$

3. Model evaluation and selection

Since height-resolved chemical flux measurements were not available at Coweeta Forest, we used the sensible heat as a proxy to evaluate how well the three inverse models (EUL, LNF, and LSM) performed in calculating the vertical distribution of scalar fluxes within the canopy. The three inverse models, along with the measured temperature profiles and turbulence statistics, were used to estimate the sensible heat flux (H) within canopy, which was compared with the sonic- anemometer-based eddy correlation measurements at different heights.

The six aspirated thermocouples, which were used to measure temperature profiles, were collocated at a common height for comparison prior to the model evaluation experiment. A total of 49 hourly measured values were recorded during June 28 – 30, 2016. Fig. S8 presents the hourly mean (±standard deviation) values of the six thermocouple measurements. The relative dispersion of the thermocouple measurements for the same hour can be expressed by the coefficient of variation (CV, standard deviation divided by the mean), which ranged from 0.12 - 1.94% with a mean value of 0.34% in the colocation experiment. The measurement bias of a particular thermocouple sensor is defined as the deviation of its recorded value from the mean of the six thermocouple measurements. Fig. S9 shows the normal quantile-quantile (Q-Q) plot of the measurement bias for each thermocouple. The points in the Q–Q plot approximately follow the 1:1 line when the biases were small but deviated when they were large. This deviation indicates that the measurement biases did not follow a normal distribution and were not likely independently random. Table S3 shows that the measurement biases were significantly correlated with the mean temperature suggesting that the temperature measurement correction should consider the magnitude of the measured temperature. Table S4 lists the regression coefficients between the individual thermocouple measurement and the mean value. Those regression coefficients were applied to correct the temperature measurement for each individual thermocouple ($T_{corrected} = b_0 + b_1 T_{raw}$) and the corrected mean air temperature profiles were used in the inverse model evaluation experiment.

The evaluation experiment was conducted during the period of July 20 to September 24, 2016. The runs were screened to eliminate the

influence of periods associated with instrumental and measurement problems or inappropriate meteorological conditions, according to the following criteria: (1) no data gap; (2) no detectable precipitation; (3) u_* measured above the canopy exceeds 0.15 m s^{-1}; (4) H measured above the canopy exceeds 20 W m^{-2}; and (5) the mean wind direction was between 40° and 85° from north and between 230° and 310° from north (minimizing the influence due to the relation between the local topographic slope and the wind angle of attack, see Novick et al. (2014)). Overall, 129 runs during the study period satisfied the above criteria and were selected for the following analysis, each representing a 60-minute sampling duration.

Fig. 1 compares the modeled sensible heat flux profiles by the three inverse models against the sonic measurements. As mentioned above, the EUL model requires two empirical constants (C_4 and C_8), the values of which are still very uncertain. Previous studies (Katul and Albertson, 1999; Siqueira et al., 2000; Ueyama et al., 2014) reported a value varying from 2 to 5 for C_4 and a value of 9 for C_8 at forest sites. For Coweeta Forest, we found that the EUL model best matched the measurements with values of 1.1 and 9 for C_4 and C_8, respectively (Fig. 1a). These constants were kept unchanged for the chemical source/sink modeling by EUL in Section 4.2. It is worth noting that these coefficients are sensitive to the definition and/or estimation of the relaxation or decorrelation time scale τ between the vertical velocity and the scalar concentration fluctuations. The work here assumes that τ may be determined from the decorrelation time of the vertical velocity fluctuations and thus can be estimated from the autocorrelation of vertical velocity (ρ_E).

In contrast to the EUL model, the Lagrangian models (LNF and LSM) produced a substantial heat sink in the lower canopy ($< 0.4\ h_c$) that was not observed in the sonic anemometer heat flux measurements. In the upper canopy, all of the models produced heat sources (positive strength), indicating transfer of heat from the upper canopy to the atmosphere. Fig. 1a shows that the Lagrangian models largely underestimated the above canopy heat flux compared to the measurements. The Lagrangian models calculate the above canopy heat flux by integrating the heat source/sink from forest floor to canopy top and the negative heat strength within the lower canopy therefore reduces the net heat flux above canopy.

The Eulerian and Lagrangian approaches differ in the treatment of vertical velocity skewness ($\overline{w'w'w'}$); EUL allows for nonzero vertical velocity skewness (Eq. (5)) while the Lagrangian approaches do not incorporate vertical velocity skewness variation, perhaps making them ill-suited for strongly skewed turbulent flows. We tested the sensitivity of modeled source-sink and flux profiles to the skewness by setting ($\overline{w'w'w'}$) to zero in the EUL. Under this condition EUL produced similar heat sinks in the lower canopy to the Lagrangian approaches and larger heat source in the upper canopy (Fig. 1a and b), indicating significant sensitivity to skewness. This result differs from the finding by Katul and Albertson (1999) that the EUL computed sources-sinks and fluxes of CO_2 were not sensitive to the vertical velocity skewness at Duke Forest. Unlike the complex topography at Coweeta Forest, Duke Forest has small local topographic variations (< 5% slopes) and the impact of skewness on vertical turbulent transport is likely negligible (Katul et al., 1999). Fig. 1c shows the scatterplot comparison of the hourly measured and EUL-calculated (includes skewness) heat fluxes at the level above canopy. The EUL sensible heat fluxes agreed well with the sonic measurements in magnitude and hour-to-hour variations, having a slope of 1.08 and a correlation coefficient of 0.64.

The model evaluation results above indicate that significant vertical skewness over complex topography can be problematic for the Lagrangian approaches and they are thus excluded in the inversion of the chemical source-sinks and fluxes. The modeled chemical source-sinks and fluxes below were solely from the EUL model in which the vertical velocity skewness was incorporated.

4. Results and discussion

4.1. Profiles of chemical concentrations

Fig. 2 presents the profiles of chemical concentrations for the measured reactive N and S compounds. The gaseous and particulate compounds all showed an overall decreasing trend from the atmosphere above canopy to the forest floor, with varied rates of decrease ($\Delta c/\Delta z$).

HNO_3 and SO_2 concentrations at the lowest level ($z/h_c = 0.018$) decreased by ~ 80% and 60%, respectively, compared to the highest level ($z/h_c = 1.26$) (Fig. 3). The mean concentration of NH_3 also decreased with height in the upper canopy but increased below the understory toward the forest floor, indicating deposition to vegetation and emission from the ground. The mean NH_3 concentrations at the bottom were still lower than that above canopy (by ~30%), showing that the NH_3 emitted from the ground (i.e., soil and/or decaying leaf litter) can be recaptured by the over-lying canopy. By examining the individual NH_3 concentration profiles, we found that 47 out of the total 76 (~62%) followed the same pattern with the mean concentration profile but the others reflected a continued decreasing trend to the forest floor (Fig. 4a), indicating that the ground acted as both a source (emission) and a sink (deposition). Comparison of the meteorological conditions associated with these two types of 'canonical profiles' showed gradients indicative of emission tended to occur at higher soil temperatures (Fig. 4b). Higher soil temperature leads to larger emission potential and compensation point of NH_3 at the surface (Massad et al., 2010; Nemitz et al., 2001). When the compensation point is above the ambient concentration near the surface, emission of NH_3 from the

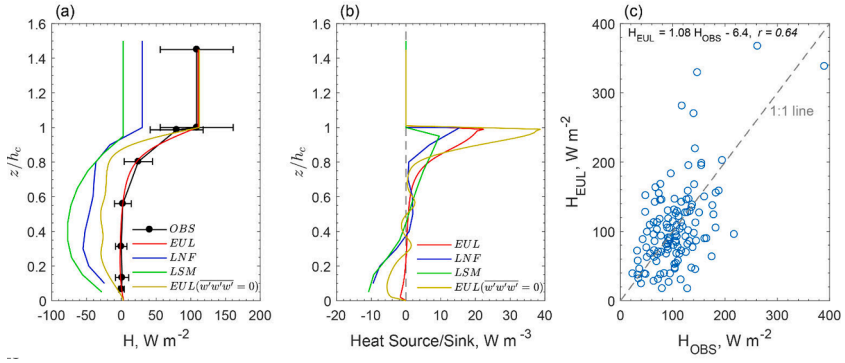

Fig. 1. (a) Comparison between observed (OBS) and modeled sensible heat flux profiles (H) by the Eulerian high-order closure model (EUL), Lagrangian localized near-field (LNF), and Lagrangian stochastic model (LSM); (b) Modeled heat sources/sinks by EUL, LNF, and LSM; (c) Scatter plot of observed and EUL-modeled sensible heat fluxes above canopy. z is height above the forest floor, and h_c is mean canopy height (=30 m). EUL($\overline{w'w'w'} = 0$) indicates EUL runs when ignoring $\overline{w'w'w'}$.

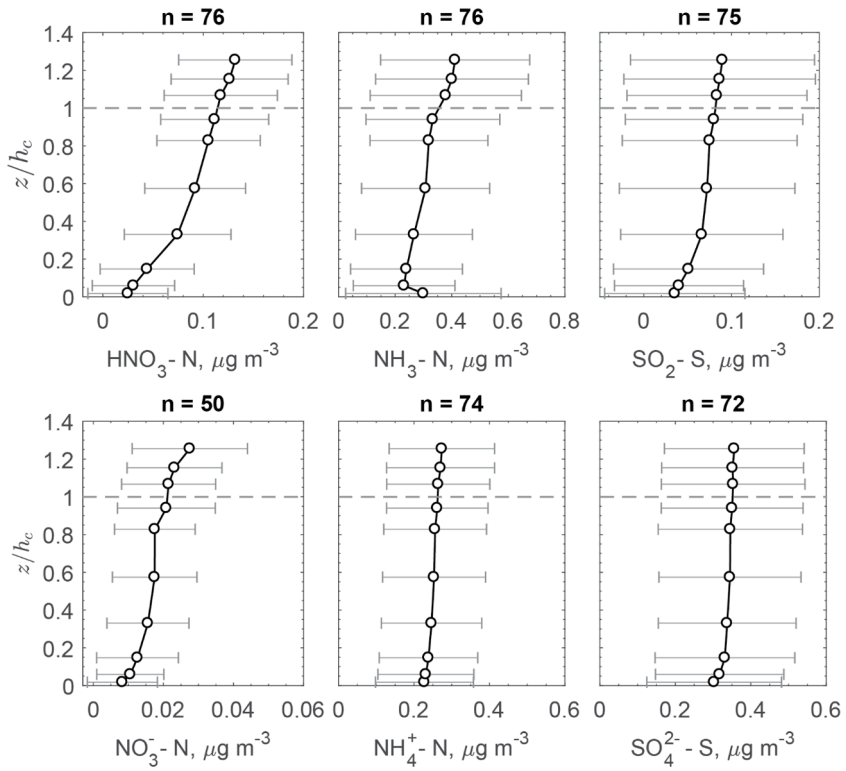

Fig. 2. Mean (±standard deviation) concentration profiles of nitric acid (HNO_3), ammonia (NH_3), sulfur dioxide (SO_2), nitrate (NO_3^-), ammonium (NH_4^+), and sulfate (SO_4^{2-}) measured during the five intensive sampling campaigns. n is sample number, z is height above the forest floor, and h_c is mean canopy height (=30 m).

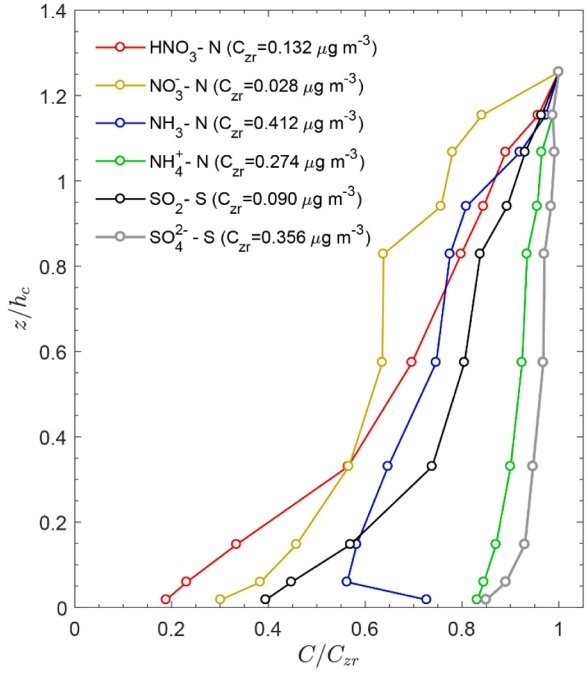

Fig. 3. Normalized mean concentration profiles of nitric acid (HNO_3), ammonia (NH_3), sulfur dioxide (SO_2), nitrate (NO_3^-), ammonium (NH_4^+), and sulfate (SO_4^{2-}) as a function of normalized height (z/h_c) measured during the five intensive sampling campaigns. C_{zr} is the concentration measured at the reference height (=37.65 m).

surface occurs and would result in the observed increase in concentration toward the ground. In addition, lower ambient concentration would also favor the occurrence of emission instead of deposition. Fig. 4a shows that the NH_3 concentrations were generally lower when an increasing trend toward the forest floor was observed (ground emission likely occurred). We note that humidity driven adsorption processes may also play a role in NH_3 exchange with the forest floor, though data were not available during the study period to assess relationships between near surface gradients of RH and NH_3.

Similar to gasses, particle concentration profiles decreased from above the canopy to the forest floor (Fig. 2). The particulate $NH_4^+$and SO_4^{2-} decreased at a lower rate within the canopy, compared to the gaseous compounds (HNO_3, SO_2, NH_3), penetrating the canopy with less than 20% loss of concentration at the measurement level closest to the forest floor (Fig. 3). Compared to $NH_4^+$and SO_4^{2-}, the canopy was a more effective sink for NO_3^- and the concentration nearest the ground was reduced by about 70% compared to that above canopy. Differing slopes for particle concentration profiles indicate differences in deposition velocity (V_d), which is a function of particle size. Zhang et al. (2008) measured the size-segregated particulate inorganic ions at Canadian rural sites and reported that the size distributions of $NH_4^+$and SO_4^{2-} peaked at 0.3–0.6 μm in diameter while NO_3^- peaked at much larger sizes (4.0–7.0 μm). Reviews of field measurements show that V_d to forest canopies generally increase with an increase of particle size for particles larger than 0.2 μm (Hicks et al., 2016; Zhang and Vet, 2006). Thus, NO_3^-would be expected to deposit faster, i.e., display a larger profile slope, if more mass was present in the > 0.2 μm fraction compared to $NH_4^+$and SO_4^{2-} .

4.2. Source, sink and chemical flux profiles

Using the measured mean concentration and velocity statistics profiles, the source-sink and flux profiles of reactive N and S compounds were estimated using the EUL model with non-zero skewness.

Walker et al., 2023 developed a V_d dataset for HNO_3 and NH_3 at Coweeta Forest for the 5th measurement intensive using the modified Bowen Ratio (MBR) method. Fig. 5 compares the V_d for HNO_3 and NH_3

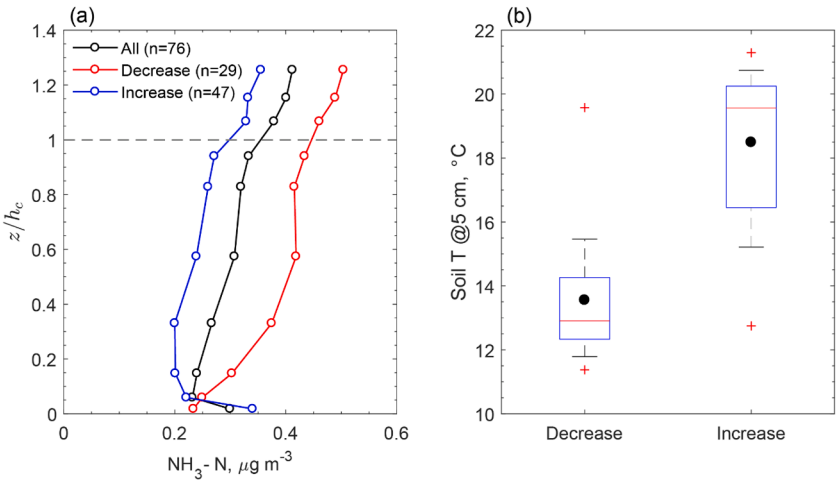

Fig. 4. (a) Mean concentration profiles of ammonia (NH_3) for all runs, and separated into subgroups of concentration profiles showing decreasing (deposition) versus increasing trend (emission) toward the forest floor; (b) Boxplot of soil temperature at a depth of 5 cm for subgroups of concentration profiles showing decreasing versus increasing trendtoward the forest floor. In each box, the central mark is the median, the ends of the box are the 25th and 75th percentiles, and the whiskers extend to the 10th and 90th percentiles. The filled circles represent the arithmetic mean and the cross symbols are the minimum and maximum values. z is height above the forest floor, and h_c is mean canopy height (=30 m).

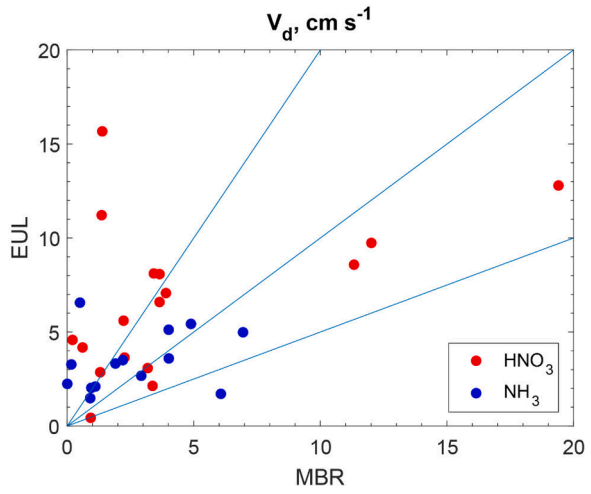

Fig. 5. Comparison of dry deposition velocity (V_d) for HNO_3 and NH_3 between the EUL inverse modeling and the modified Bowen Ratio (MBR) method during the 5th measurement intensive. Reference lines of 1:2, 1:1 and 2:1 are shown.

between the EUL inverse modeling and the MBR method. The EUL V_d was calculated from the EUL modeled flux above the canopy scaled with the concentration at the reference height ($V_d = F/C_{zr}$) used by Walker et al., 2023. Most of the points fall within or close to a factor of 2, indicating reasonable agreement between the EUL model and the MBR measurement, particularly given the uncertainties of estimating V_d in both methods and the limited sample sizes ($n = 17$ for HNO_3 and $n = 14$ for NH_3).

As is common in micro-meteorology, the source-sink density profiles display the vertical distribution of deposition (negative) and/or emission (positive) within the canopy layers. The largest deposition of HNO_3–N occurred in the uppermost part of the canopy with a sink strength up to $-3.0\ \mu g\ m^{-3}\ h^{-1}$ (upper panel in Fig. 6). A second peak of HNO_3–N sink occurred close to the ground resulting from the effective uptake by the forest floor, though the sink strength was much smaller ($-0.21\ \mu g\ m^{-3}\ h^{-1}$) compared to the upper canopy due to weaker turbulent mixing (i.e., reduced vertical velocity variance) and smaller depositional surface area. Flux profiles can be computed by integrating the source-sink profiles from the forest floor to the canopy top (the lower panel in Figs. 6-8). The HNO_3–N flux profile showed a monotonically increasing trend in magnitude from the forest floor to the canopy top due to the accumulated uptake by the canopy elements. The average flux of HNO_3–N above the canopy was $-27.15\ \mu g\ m^{-2}\ h^{-1}$.

In Section 4.1, we found that the average NH_3 concentration increased toward the forest floor, which is different from the monotonically decreasing patterns exhibited by the other reactive compounds (Fig. 2). Fig. 6 shows that the source-sink profile of NH_3–N exhibited emission with a small strength up to $0.18\ \mu g\ m^{-3}\ h^{-1}$ close to the ground (an enlarged plot was shown in Fig. S10), turning to a sink (negative) above $0.16\ h_c$, and peaking at a sink strength of $-8.7\ \mu g\ m^{-3}\ h^{-1}$ close to the canopy top. The average flux profile of NH_3–N indicated a small net emission (positive flux) below $0.33\ h_c$, reaching a maximum up to $0.52\ \mu g\ m^{-2}\ h^{-1}$, and net deposition (negative flux) above. The forest was overall a net sink of NH_3–N with a deposition flux of $-70.0\ \mu g\ m^{-2}\ h^{-1}$ above the canopy top. As shown in Fig. 4, although the average NH_3 concentration increased toward the forest floor, the individual NH_3 concentration profiles may present an increasing or a decreasing trend towards the forest floor under different environmental conditions. When the NH_3 mean concentration exhibited monotonically decreasing patterns from above the canopy to the forest floor, only deposition occurred and the shape of the NH_3 source-sink profiles was similar with that of HNO_3 (Fig. 7). When environmental conditions favored emission of NH_3 from the ground (e.g., higher soil temperature), the mean concentration increased toward the forest floor and the model estimated a NH_3–N emission from the ground with a source strength up to $0.95\ \mu g\ m^{-3}\ h^{-1}$, which was, however, still much smaller than the sink strength at the upper canopy (about $-9\ \mu g\ m^{-3}\ h^{-1}$). Thus, the canopy (leaves, branches) was a sink for NH_3 but the ground can act as a source or a sink at Coweeta Forest. NH_3 emitted from the ground was relatively small and was recaptured by the over-lying canopy.

The average flux of total N (HNO_3–$N + NH_3$–$N + NH_4^+$-$N + NO_3^-$-N) above canopy was $-143.9\ \mu g\ m^{-2}\ h^{-1}$, exhibiting net deposition (sink) from the forest floor to the canopy top with maximum sink strength in the upper canopy (Fig. 6). NH_3–N made the largest contribution (48.6%), which is not surprising due to its higher concentration (see Fig. 3) relative to the other N compounds. HNO_3–N contributed 18.9% of the total N flux and particulate compounds (NH_4^+-N + NO_3^--N) together contributed 32.5%, reflecting smaller contributions than the gaseous species.

The forest was also a net sink for reactive S compounds, with source-sink profiles of SO_2-S and SO_4^{2-}-S both showing strong uptake in the upper canopy. The sink strengths of SO_2-S and SO_4^{2-}-S were similar at Coweeta Forest and the averaged fluxes above the canopy were ~ $-12.0\ \mu g\ m^{-2}\ h^{-1}$ for SO_2-S and SO_4^{2-}-S, contributing similarly to the total S flux (Fig. 8). While concentration profiles indicate slower deposition of SO_4^{2-}-S compared to SO_2-S (Fig. 3), SO_4^{2-}-S concentrations were a factor of 4 larger (Fig. 2).

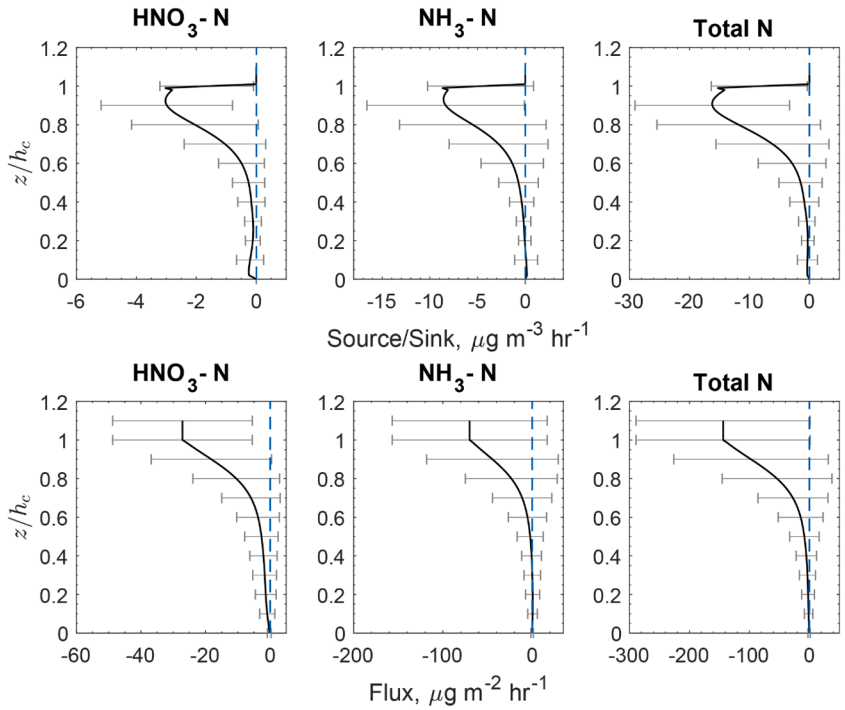

Fig. 6. Source/sink (upper panel) and flux (lower panel) profiles for HNO_3 - N, NH_3 - N, and total N modeled by EUL during the five intensive sampling campaigns. Note that total $N = HNO_3$ - $N + NH_3$ - $N + NH_4^+$- $N + NO_3^-$- N. Solid lines represent the mean values of the sampled concentration profiles (sample size shown in Fig. 2). Error bars indicate the standard deviation from the mean. z is height above the forest floor, and h_c is mean canopy height (=30 m).

4.3. Partitioning to canopy compartments

In an effort to offer plausibility arguments about the key physical, chemical, or biological processes responsible for the source-sink strength at a given z, the relation between Source-Sink and the canopy leaf area density for differing environmental and edaphic conditions are analyzed.

According to the vertical distribution of leaf area density at Coweeta Forest (Fig. S11), the canopy can be divided into three compartments: crown ($> 0.6h_c$), middle canopy (0.2 - $0.6h_c$), and understory ($< 0.2h_c$). Source-sink profiles were integrated to derive the fractions of total N and S deposition to specific canopy compartments. As shown in Table 1, ~ 80–90% of reactive N and S compounds deposited in the crown area. The middle canopy and understory received similar fractions of deposited N and S, on the order of 10% or less. As the ground emitted NH_3 under some circumstances, offsetting NH_3 uptake within the lower canopy, the net deposition flux of NH_3 integrated within the understory region was small (~ 0.7% to the total net flux). The dominant role of the crown foliage (external surfaces and stomata) to the canopy-scale flux is attributed to higher air concentrations and stronger turbulent exchange (smaller resistances) near the canopy top. Covering April to October, the five measurement intensives can be divided into Spring, Summer, and Fall to examine seasonal differences. Table S5 shows that the partitioning to canopy compartments is similar across seasons, further supporting the conclusion from Table 1 that crown foliage dominates the uptake of reactive N and S compounds during the growing season at Coweeta Forest.

The dry deposition modules widely used in chemistry transport models (CTM) and deposition monitoring networks are developed and evaluated based on above-canopy flux measurements (Flechard et al., 2011; Wesely and Hicks, 2000; Wu et al., 2018). Parameters for different exchange pathways (stomata, cuticle, ground) can be tuned to optimize agreement between the modeled and observed above-canopy flux. The partitioning fractions listed in Table 1 can be used to independently assess and constrain the relative contribution of individual exchange pathways in resistance-based dry deposition models.

In the SANDS study, Walker et al. (2023) modeled the exchange fluxes of reactive compounds at Coweeta Forest using the Surface Tiled Aerosol and Gaseous Exchange (STAGE) model used in the Community Multi-scale Air Quality Model (CMAQ) version 5.3. The STAGE model parameterizes the air-surface exchange of gas as a gradient process following Nemitz et al. (2001) and Massad et al. (2010). At a vegetated site, the component fluxes are calculated as following:

$$F_s = -\frac{\chi_c - \chi_s}{R_s}, \tag{15}$$

$$F_{cut} = -\frac{\chi_c - \chi_{cut}}{R_{cut}}, \tag{16}$$

$$F_g = -\frac{\chi_{z_0} - \chi_g}{R_g}, \tag{17}$$

where F_s, F_{cut}, and F_g are the component flux to leaf stomata, leaf cuticle, and ground surface, respectively. The net flux over canopy is the sum of the component fluxes ($F_{net} = F_s + F_{cut} + F_g$). R_s, R_{cut}, and R_g are the stomatal, cuticular, and total ground resistances, respectively. χ_{z_0} is the concentration at height displacement height + roughness length and χ_c, χ_s, χ_{cut}, and χ_g are the canopy, stomatal, cuticular, and ground compensation points, respectively. More details about the model formulations and configuration are provided in Bash (2023) and Walker et al. (2023). The STAGE model calculates the deposition velocity for particles following the single big-leaf approach and does not estimate the component flux to different canopy elements.

Table 1 summarizes the proportions of the component fluxes (stomata, cuticle, and ground) to the total net flux from the STAGE model for the same periods and inputs (air concentrations, turbulence measurements) as the EUL simulations. The sources/sinks of reactive N and S within the crown and middle canopy areas should mainly be attributed to the interactions with leaves (external and internal surfaces), so the EUL calculated flux within crown and middle canopy areas can be linked with the stomatal and cuticular component fluxes by STAGE. The STAGE ground flux can be compared with the EUL flux below the understory in

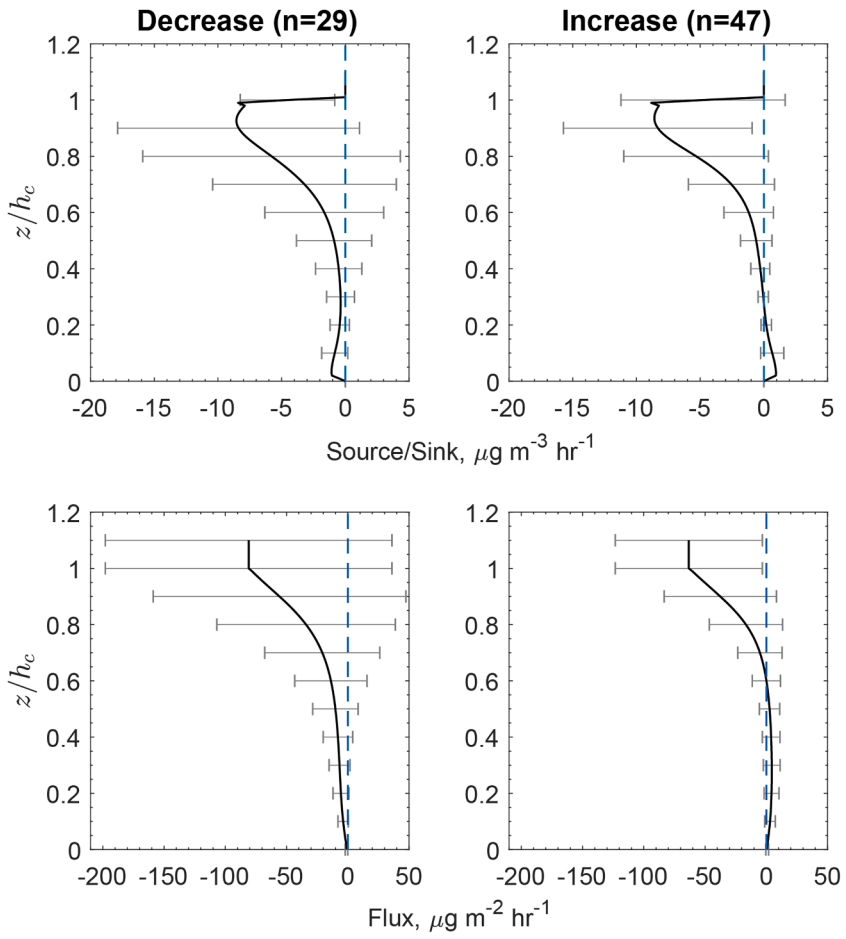

Fig. 7. Source/sink (upper panel) and flux (lower panel) profiles of NH_3 - N modeled by EUL for a subgroup of concentration profiles showing decreasing trend toward the forest floor (left panel), and a subgroup of concentration profiles showing increasing trend toward the forest floor (right panel). z is height above the forest floor, and h_c is mean canopy height (=30 m).

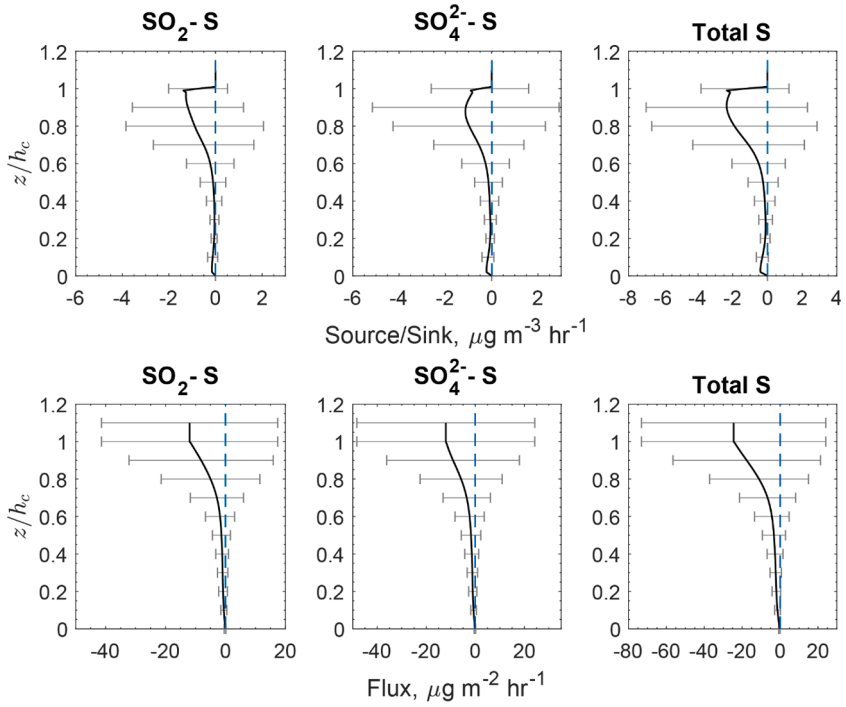

Fig. 8. Same as Fig. 5, but for SO_2 - S, SO_4^{2-} - S, and total S. Note that total $S = SO_2$ - $S + SO_4^{2-}$ - S.

Table 1
Partitioning of deposited reactive N and S compounds to canopy compartments (%) estimated by EUL and to the canopy elements estimated by STAGE.

Model	Compartment	HNO_3 - N	NH_3 - N	NO_3^- - N	NH_4^+ - N	Total N	SO_2 - S	SO_4^{2-} - S	Total S
EUL	Crown (>0.6h_c)	86.3	92.6	89.9	89.0	89.9	84.7	80.5	82.4
	Middle canopy (0.2–0.6h_c)	8.8	8.1	7.5	8.7	8.6	8.4	10.8	9.6
	Understory (<0.2h_c)	4.9	−0.7[a]	2.5	2.3	1.5	6.8	8.7	8.0
STAGE	Stomata	0.4	7.3	–	–	–	32.8	–	–
	Cuticle	93.8	86.8	–	–	–	46.4	–	–
	Ground	5.8	5.9	–	–	–	20.8	–	–

[a] The negative sign indicates the flux integrated within the understory (upward) is opposite in direction to the net flux above canopy (downward).

which the sources/sinks are mostly from the ground.

For HNO_3, which has small non-stomatal resistance, STAGE predicted that 93.8% of the flux is through the cuticular pathway. Only 0.4% was attributed to the stomatal uptake, likely due to the large resistance for the molecular diffusion through stomata. Based on the STAGE modeling, 94.2% of deposited HNO_3 was attributed to leaves (stomata + cuticle) and 5.8% to the ground surface, which was comparable to the partitioning estimated from the EUL calculations (95.1% in crown and middle canopy, 4.9% in understory). STAGE also predicted that flux to the foliage dominated the total fluxes of NH_3 and SO_2 (94.1% and 79.2%, respectively) but the contributions of ground fluxes were larger than the estimates based on the EUL fluxes (5.9 % vs −0.7% for NH_3 and 20.8 % vs 6.8% for SO_2). STAGE incorporates ground and foliage emission potentials of NH_3, which can impact the direction (upward or downward) of the modeled fluxes. The EUL-calculated fluxes showed that 47 of the total 76 NH_3 samples resulted in NH_3 emissions from the ground (Fig. 7) as the NH_3 concentrations were observed to increase toward the forest floor. However, STAGE only produced NH_3 ground emissions for 9 of the 47 samples, which indicated a potential underestimation of NH_3 ground emission and thus an overestimation of deposition to the ground. Uncertainties in specifying NH_3 emission potentials for soil and litter may be a source of bias in the NH_3 ground fluxes predicted by STAGE. The total ground resistance (R_g) controls the air-soil exchange and is the sum of the in-canopy aerodynamic resistance (R_{inc}), ground boundary layer resistance (R_{bg}), and soil resistance (R_{soil}) ($R_g = R_{inc} + R_{bg} + R_{soil}$). HNO_3 has a small R_{soil} due to the tendency to absorb onto external surfaces and its ground flux is limited by R_{inc} and R_{bg}. Good agreement between the EUL inverse and STAGE modeled ground HNO_3 flux suggests reasonable estimates of R_{inc} and R_{bg} in STAGE. For SO_2, R_{soil} is a dominant component of R_g. Thus, overestimation of SO_2 deposition to the ground compared to EUL could result from an underestimation of R_{soil} for SO_2 in STAGE.

Besides the vertical partitioning of the fluxes, it is also interesting to compare the magnitudes of flux estimated by EUL and STAGE. As shown in Fig. 9, the above-canopy fluxes of HNO_3 estimated by the two approaches were comparable while significant differences were observed in the fluxes of NH_3 and SO_2. In STAGE, HNO_3 flux (or V_d) is governed by the aerodynamic (R_a) and quasi-laminar resistances (R_b) as its surface resistance (R_c) is generally small if not negligible (Meyers et al., 1989; Wu et al., 2021). For SO_2 and NH_3, R_c is dominant in the deposition process as it is typically much larger in magnitude than R_a and R_b (Wesely and Hicks, 2000). The NH_3 flux is bi-directional and requires parameterizations for the compensation points (Flechard et al., 2013; Zhang et al., 2010). R_a and R_b can be estimated using the conventional micrometeorological approaches based on similarity theory above the canopy. The parameterizations for R_c and compensation points are complex and subject to large uncertainties that are likely to be the main source of uncertainties for the STAGE-estimated flux of NH_3 and SO_2.

4.4. Flux uncertainty due to concentration measurement errors

One of the main criticisms of the EUL inverse model is its sensitivity to concentration measurement errors as EUL does not utilize any redundancy in concentration profiles (Katul and Albertson, 1999). As shown in Section 2.2, the relative errors of the concentration

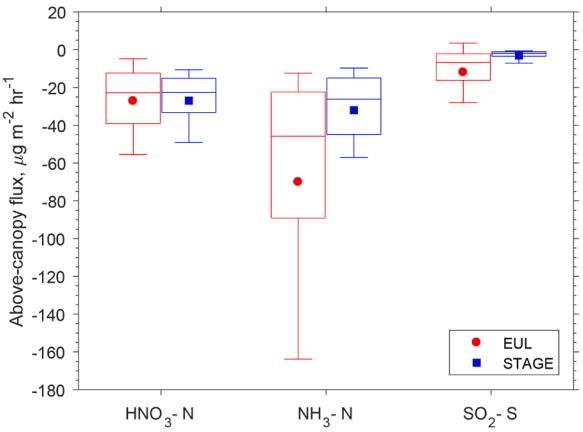

Fig. 9. Comparison of the estimated above-canopy fluxes of HNO_3 - N, NH_3 - N, and SO_2 - S between EUL and STAGE. In each box, the central mark is the median, the ends of the box are the 25th and 75th percentiles, and the whiskers extend to the 10th and 90th percentiles. Filled circles/squares represent the arithmetic mean.

measurements for the reactive N and S compounds followed approximately normal distributions with mean values of −2.74 to 4.65%, varying with chemical species (see Table S2 and Figs. S2 – S7). Based on the assumption that the random measurement errors are normally distributed, a total of 10,000 Monte Carlo simulations were generated. For every simulation, each of the measured concentrations was perturbed with a randomly sampled relative error:

$$C'_{i,j,k} = C_{i,j,k} \times (1 + \delta_i), \quad (18)$$

where $C'_{i,j,k}$ is the perturbed concentration for the *ith* species, *jth* profile, and *kth* vertical level and C is the corresponding measured values. The δ_i is the relative measurement error for the *ith* species, randomly sampled based on the distribution parameters listed in Table S2.

For each Monte Carlo simulation, the source-sink and flux profiles for each reactive N and S profile were calculated and then averaged for the study period. Figs. 10-11 display the means and standard deviations of the source-sink and flux profiles from the Monte Carlo simulations (n = 10,000). The mean source-sink and flux profiles of the Monte Carlo simulations were close to the results in Section 4.2 (no perturbation in concentration) in magnitude and shape. The fluxes at a particular height from the 10,000 simulations followed normal distributions (Figs. S12-S14), with large variations from the mean values. The flux uncertainties can be estimated as two times of the standard deviation (2σ) of the 10,000 simulations. Table 2 summarizes the relative flux uncertainties (uncertainty divided by the mean) at the concentration measurement heights. The above-canopy fluxes of reactive N compounds exhibited an uncertainty of 227–289%, lower than that for the reactive S compounds (459–693%). Fluxes in the lower canopy generally (except NH_3 and NH_4^+) had smaller relative uncertainties than those in the upper canopy. This difference is likely to be due to the weaker turbulence in the lower canopy that produced smaller source/sink strengths for the same

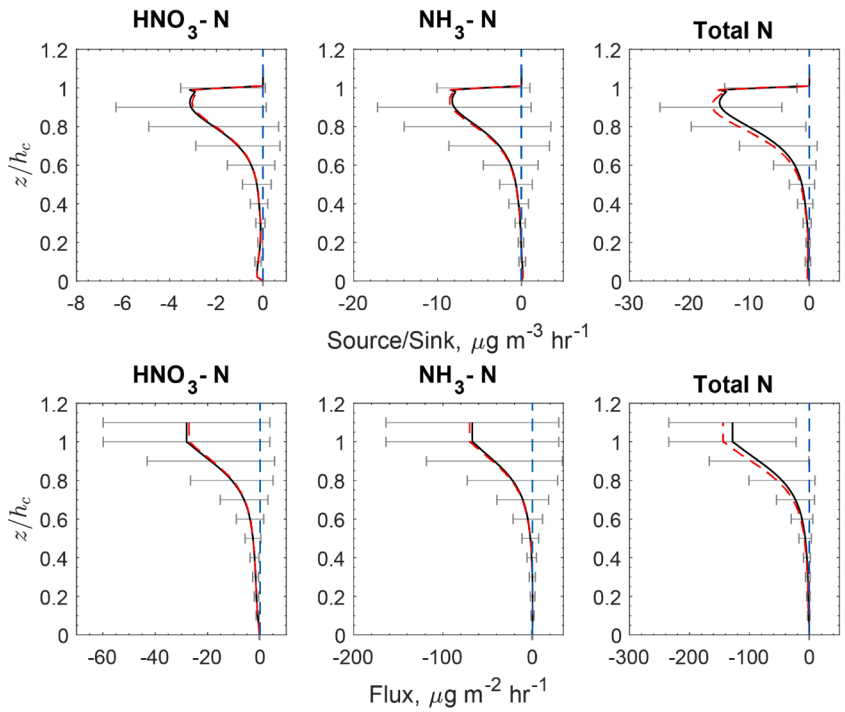

Fig. 10. Source/sink (upper panel) and flux (lower panel) profiles for HNO_3 - N, NH_3 - N, and total N modeled by EUL in the Monte Carlo simulation. Solid lines represent the mean values of the 10,000 simulations. Error bars indicate the standard deviation from the mean. Dashed red lines are the mean values of the base simulations (see Fig. 6). z is height above the forest floor, and h_c is mean canopy height (=30 m).

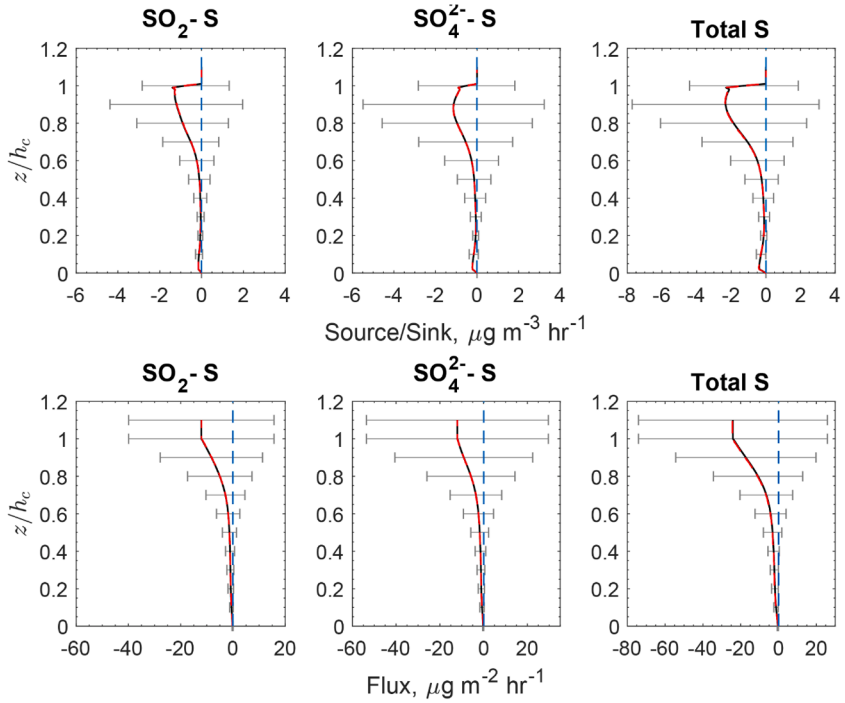

Fig. 11. Same as Fig. 10, but for SO_2 - S, SO_4^{2-} - S, and total S. Note that total $S = SO_2$ - $S + SO_4^{2-}$ - S.

concentration gradients in the upper canopy. As the soil/litter layer may emit NH_3, the overlapping of emission sources and deposition sinks in the lower canopy resulted in large variations and small mean values in the NH_3 fluxes and thus large relative uncertainties. The soil/litter NH_3 emission could reduce the NH_4^+concentration gradient in the lower canopy through gas-particle partitioning, which then leads to small NH_4^+fluxes and large relative flux uncertainties.

5. Conclusions and recommendations

The vertical distribution of sources/sinks and fluxes within vegetation canopies is a pre-requisite to understanding air-vegetation exchange processes of reactive compounds and identification of the dominant source/sink pathways. The present study implemented three inverse models (EUL, LNF, and LSM) to calculate vertical flux and

Table 2
Relative uncertainties (%) of the EUL calculated fluxes based on the Monte Carlo simulations (relative uncertainty = 2 × standard deviation / mean × 100%).

Level	HNO_3 - N	NH_3 - N	NO_3^- - N	NH_4^+ - N	Total N	SO_2 - S	SO_4^{2-} - S	Total S
$> h_c$	227	289	242	256	166	459	693	415
$0.94h_c$	248	333	268	271	186	472	695	426
$0.83h_c$	287	439	331	309	233	486	696	435
$0.57h_c$	254	745	317	386	296	456	534	362
$0.33h_c$	137	937	188	345	287	280	287	202
$0.15h_c$	125	913	174	373	367	251	266	186
$0.06h_c$	127	924	169	387	379	236	265	182
$0.02h_c$	120	984	159	382	289	220	273	178

Note: h_c refers to the mean canopy height (=30 m).

source-sink profiles from scalar concentration profiles at a mixed forest canopy. The ability of the three models to calculate vertical fluxes was evaluated against multi-level eddy-covariance measurements of sensible heat flux. The inverse models following the Lagrangian or Eulerian frameworks performed differently at Coweeta Forest. The Eulerian higher-order closure model, with its ability to incorporate vertical velocity skewness performed well in estimating the sensible heat flux profiles. The examined Lagrangian approaches, which do not allow for non-zero vertical velocity skewness, failed to capture the vertical distribution of sensible heat flux compared to the measurements. This finding indicates that the skewness of the vertical velocity cannot be ignored at this site.

The Eulerian higher-order closure model, which also produced comparable dry deposition velocities of HNO_3 and NH_3 against the modified Bowen Ratio (MBR) measurements, was subsequently used to calculate the source-sink and flux profiles of reactive N and S compounds. The source-sink and flux profiles showed that, different from the canopy elements (leaves, branches) that always act as a sink for NH_3, the soil/litter layer can also emit NH_3. Soil temperature was shown to play a key role in the release or uptake of NH_3 from the ground surface. The NH_3 emitted from the ground was relatively small in strength and was rapidly recaptured by the over-lying canopy. Overall, the forest was a net sink for NH_3. The other species (i.e., HNO_3, SO_2, NO_3^-, NH_4^+, SO_4^{2-}), which exhibit a unidirectional (deposition) exchange, display bimodal sink profile distributions with one large peak in the crown area and another much smaller mode near the ground. The majority (80–90%) of reactive N and S compounds deposited in the crown region (> 60% canopy height) with only a small fraction (<10%) depositing to the understory region including soil/litter. Mainly due to its higher ambient concentration compared to the other N compounds, the NH_3 flux comprised about half of the total reactive N deposited to the canopy. For reactive S, the contributions of gaseous (SO_2) and particulate (SO_4^{2-}) compounds were similar. Uncertainties in above-canopy fluxes derived from Monte Carlo analysis ranged from 227 to 289% for reactive N compounds and of 459–693% for the reactive S compounds. The large flux uncertainties can be attributed to the lack of redundancy in the inversion for source/sink strength from measured concentrations in the EUL framework and the low N and S concentrations observed at Coweeta Forest.

The resistance-based STAGE model showed reasonable agreement with the inverse model (EUL) in magnitude of estimated above-canopy flux and partitioning within the canopy for HNO_3. Larger differences between the two models were found for SO_2 and NH_3, which require more complex parameterizations to represent the surface resistance, exchange with the ground layer, and NH_3 compensation points. The comparison indicates that those processes may need to be refined for the STAGE model. Regarding extension of source-sink modeling of reactive N and S in forest canopies, further comparison of Eulerian and Lagrangian approaches in more ideal terrain is needed to assess the representativeness of model performance at Coweeta. Assessment of source-sink profiles across a wider range of LAI and atmospheric concentrations is also needed to inform seasonality in partitioning of fluxes between the canopy and ground and to assess inverse model sensitivity to measurement uncertainty.

The results here show the vast majority of dry deposition occurs in the canopy crown during the growing season, even for slow depositing particles. In the context of total wet + dry deposition, this means that different vegetation species in forests with closed canopies similar to Coweeta Forest are exposed to atmospheric compounds by differing deposition pathways. Crown tree species receive a larger portion of direct exposure from dry deposition compared to understory and ground-dwelling species, whereas the latter receive the majority of exposure from throughfall, which is wet deposition chemically modified by transformation, uptake, and leaching during transit through the canopy. The implications of wet versus dry partitioning with respect to critical loads and response to exposure will differ among species. Epiphytic lichen, which have no roots and derive nutrients directly from deposition of material to their thallus surface, have long been considered bioindicators of ecosystem risk to air pollution and the subject of much research on critical loads of nutrients and acidity (Jovan et al., 2012). Studies show that lichen community response to deposition is more dramatic when exposure occurs via dry deposition (Carter et al., 2017), as accumulated material becomes highly concentrated at the onset of surface moisture (e.g., dew, fog, precipitation). Thus, in closed forest canopies, lichen communities below the crown receiving a critical load of N or S from wet throughfall may be expected to respond differently to the same amount of total deposition in an open canopy forest where lichen receive a larger portion of exposure from dry deposition. Deposition budgets (i.e., speciated wet + dry) derived from CTMs or measurement-model fusion approaches reflect inputs to the top of the canopy. Subsequently, corresponding estimates of critical load exceedance for below-crown species cannot distinguish between wet versus dry pathways, confounding interpretation of ecosystem risk. Vertically resolved in-canopy sources and sinks are needed to elucidate such details and inform ecological assessments. To what degree they will replace resistance-based formulations remains a future question for CTMs.

Declaration of Competing Interest

The authors declare that they have no known competing financial interests or personal relationships that could have appeared to influence the work reported in this paper.

Data availability

Data will be made available on request.

Acknowledgments

We greatly appreciate the comments by Jonathan Pleim and Ryan Fulgham of the U.S. Environmental Protection Agency. We also acknowledge field and laboratory support from U.S. EPA staff, including Ryan Daly, Aleksandra Djurkovic, Mark Barnes, David Kirchgessner, and Lee Nanney, as well as the U.S. Forest Service staff at the Coweeta

Hydrological Laboratory, including Christine Sobek, Patsy Clinton, Chuck Marshall and Cindi Brown. The views expressed in this article are those of the authors and do not necessarily represent the views or policies of the U.S. Environmental Protection Agency or U.S. Department of Agriculture. The use of trade or firm names in this publication is for reader information and does not imply endorsement by the U.S. Environmental Protection Agency or U.S. Department of Agriculture of any product or service. This work was supported by the U.S. Environmental Protection Agency and the USDA Forest Service, Southern Research Station, Coweeta Hydrologic Lab.

Supplementary materials

Supplementary material associated with this article can be found, in the online version, at doi:10.1016/j.agrformet.2023.109386.

References

Bash, J. et al., 2023. Evaluation of HNO_3, SO_2, and NH_3 in the Surface Tiled Aerosol and Gaseous Exchange (STAGE) option in the Community Multiscale Air Quality Model version 5.3.1 against field scale, in situ and satellite observation. In preperation.

Carter, T.S., et al., 2017. Mechanisms of nitrogen deposition effects on temperate forest lichens and trees. Ecosphere 8 (3), e01717.

Currie, L.A., 1995. Nomenclature in evaluation of analytical methods including detection and quantification capabilities (IUPAC Recommendations 1995). Pure Appl. Chem. 67 (10), 1699–1723.

Denmead, O., Freney, J., Dunin, F., 2008. Gas exchange between plant canopies and the atmosphere: case-studies for ammonia. Atmos. Environ. 42 (14), 3394–3406.

Duman, T., Trakhtenbrot, A., Poggi, D., Cassiani, M., Katul, G.G., 2016. Dissipation intermittency increases long-distance dispersal of heavy particles in the canopy sublayer. Bound. Layer Meteorol. 159 (1), 41–68.

Finnigan, J.J., 1985. Turbulent transport in flexible plant canopies. In: Hutchison, B.A., Hicks, B.B. (Eds.), The Forest-Atmosphere Interaction. D. Reidel Publishing Company, Dordrecht, pp. 443–480.

Flechard, C., et al., 2013. Advances in understanding, models and parameterizations of biosphere-atmosphere ammonia exchange. Biogeosciences 10 (7), 5183–5225.

Flechard, C., et al., 2011. Dry deposition of reactive nitrogen to European ecosystems: a comparison of inferential models across the NitroEurope network. Atmos. Chem. Phys. 11 (6), 2703–2728.

Fowler, D., et al., 2009. Atmospheric composition change: ecosystems—atmosphere interactions. Atmos. Environ. 43 (33), 5193–5267.

Harper, L., Denmead, O., Sharpe, R., 2000. Identifying sources and sinks of scalars in a corn canopy with inverse Lagrangian dispersion analysis: II. Ammonia. Agric. For. Meteorol. 104 (1), 75–83.

Hicks, B.B., Saylor, R.D., Baker, B.D., 2016. Dry deposition of particles to canopies—a look back and the road forward. J. Geophys. Res. Atmos. 121 (24), 14691–14707.

Jovan, S., Riddell, J., Padgett, P.E., Nash III, T.H., 2012. Eutrophic lichens respond to multiple forms of N: implications for critical levels and critical loads research. Ecol. Appl. 22 (7), 1910–1922.

Katul, G., et al., 1999. Spatial variability of turbulent fluxes in the roughness sublayer of an even-aged pine forest. Bound. Layer Meteorol. 93 (1), 1–28.

Katul, G., et al., 1997. A Lagrangian dispersion model for predicting CO2 sources, sinks, and fluxes in a uniform loblolly pine (Pinus taeda L.) stand. J. Geophys. Res. Atmos. 102 (D8), 9309–9321.

Katul, G.G., Albertson, J.D., 1999. Modeling CO2 sources, sinks, and fluxes within a forest canopy. J. Geophys. Res. Atmos. 104 (D6), 6081–6091.

Massad, R.-S., Nemitz, E., Sutton, M., 2010. Review and parameterisation of bi-directional ammonia exchange between vegetation and the atmosphere. Atmos. Chem. Phys. 10 (21), 10359–10386.

Massad, R.S., Loubet, B., 2015. Review and Integration of Biosphere-Atmosphere Modelling of Reactive Trace Gases and Volatile Aerosols. Springer, Dordrecht, pp. 1–5.

Meyers, T., Huebert, B., Hicks, B., 1989. HNO3 deposition to a deciduous forest. Bound. Layer Meteorol. 49 (4), 395–410.

Meyers, T.P., 1987. Modelling the plant canopy micrometeorology with higher-order closure principles. Agric. For. Meteorol. 41 (1–2), 143–163.

Nemitz, E., Milford, C., Sutton, M.A., 2001. A two-layer canopy compensation point model for describing bi-directional biosphere-atmosphere exchange of ammonia. Q. J. R. Meteorol. Soc. 127 (573), 815–833.

Novick, K., Brantley, S., Miniat, C.F., Walker, J., Vose, J., 2014. Inferring the contribution of advection to total ecosystem scalar fluxes over a tall forest in complex terrain. Agric. For. Meteorol. 185, 1–13.

Novick, K., et al., 2013. Eddy covariance measurements with a new fast-response, enclosed-path analyzer: spectral characteristics and cross-system comparisons. Agric. For. Meteorol. 181, 17–32.

Oishi, A.C., et al., 2018. Warmer temperatures reduce net carbon uptake, but do not affect water use, in a mature southern Appalachian forest. Agric. For. Meteorol. 252, 269–282.

Raupach, M., 1989a. Applying Lagrangian fluid mechanics to infer scalar source distributions from concentration profiles in plant canopies. Agric. For. Meteorol. 47 (2–4), 85–108.

Raupach, M., 1989b. A practical Lagrangian method for relating scalar concentrations to source distributions in vegetation canopies. Q. J. R. Meteorol. Soc. 115 (487), 609–632.

Raupach, M.R., 1988. Canopy transport processes. In: Steffen, W.L., Denmead, O.T. (Eds.), Flow and Transport in the Natural environment: Advances and Applications. Springer-Verlag, Berlin, pp. 95–127.

Rodean, H.C., 1996. Stochastic Lagrangian Models of Turbulent Diffusion. American Meteorological Society, Boston, pp. 26.

Siqueira, M., Lai, C.T., Katul, G., 2000. Estimating scalar sources, sinks, and fluxes in a forest canopy using Lagrangian, Eulerian, and hybrid inverse models. J. Geophys. Res. Atmos. 105 (D24), 29475–29488.

Thomson, D., 1987. Criteria for the selection of stochastic models of particle trajectories in turbulent flows. J. Fluid Mech. 180, 529–556.

Ueyama, M., Takanashi, S., Takahashi, Y., 2014. Inferring methane fluxes at a larch forest using Lagrangian, Eulerian, and hybrid inverse models. J. Geophys. Res. 119 (10), 2018–2031.

Walker, J.T., Chen, X., Wu, Z., Schwede, D., Daly, R., Djurkovic, A., Oishi, A.C., Edgerton, E., Bash, J., Knoepp, J., Puchalski, M., Iiames, J., Miniat, C.F., 2023. Atmospheric deposition of reactive nitrogen to a deciduous forest in the southern Appalachian Mountains. Biogeosciences 20, 971–995. https://doi.org/10.5194/bg-20-971-2023.

Wesely, M., Hicks, B., 2000. A review of the current status of knowledge on dry deposition. Atmos. Environ. 34 (12), 2261–2282.

Wu, Z., et al., 2021. Extension of a gaseous dry deposition algorithm to oxidized volatile organic compounds and hydrogen cyanide for application in chemistry transport models. Geosci. Model Dev. Discuss. 2021, 1–31.

Wu, Z.Y., et al., 2018. Evaluation and intercomparison of five North American dry deposition algorithms at a mixed forest site. J. Adv. Model. Earth Syst. 10 (7), 1571–1586.

Zhang, L., Vet, R., 2006. A review of current knowledge concerning size-dependent aerosol removal. China Particuol. 4 (06), 272–282.

Zhang, L., et al., 2008. Characterization of the size-segregated water-soluble inorganic ions at eight Canadian rural sites. Atmos. Chem. Phys. 8, 7133–7151.

Zhang, L., Wright, L., Asman, W., 2010. Bi-directional air-surface exchange of atmospheric ammonia: a review of measurements and a development of a big-leaf model for applications in regional-scale air-quality models. J. Geophys. Res. Atmos. 115, D20310.